Object-oriented Composite Analysis of Warm Sector Rainfall in North China

Jiaolan Fu[1, 2], Fuqing Zhang[2], and Timothy D. Hewson[3]

[1]National Meteorological Center, China Meteorological Administration, Beijing, China

[2]Department of Meteorology and Atmospheric Science, and Center for Advanced Data Assimilation and Predictability Techniques, The Pennsylvania State University, University Park, Pennsylvania

[3]ECMWF, Shinfield Park, Reading, UK

Monthly Weather Review

February 10, 2019

Correspondence to: Jiaolan Fu (fujiaolan@cma.gov.cn)

Early Online Release: This preliminary version has been accepted for publication in *Monthly Weather Review*, may be fully cited, and has been assigned DOI 10.1175/MWR-D-19-0038.1. The final typeset copyedited article will replace the EOR at the above DOI when it is published.

Abstract

Warm sector rainfall (WSR) occurs, by definition, in a warm air region that is isolated from any forcing related to synoptic frontal boundaries at the surface. This study explores the use of an object-oriented technique to objectively and automatically identify various WSR events over North China from June to September in 2012-2017. A total of 768 substantive events are identified over the 6 years. They have a mean maximum rainfall accumulation of 35 mm/hr. Most such events occur over the plains; with two frequency maxima, one to the south of the Yanshan Mountain Ranges, and the other near the junction of Henan, Shandong and Jiangsu provinces. WSR-related rainstorms can form in all warm-season months but are most commonly seen between mid-July and mid-August (40% of all events occurred then). Geographically, the region at greatest risk moves gradually northward from mid-June to mid-August, consistent with the progression of the East Asian summer monsoon. There are two diurnal peaks in WSR activity, one from late afternoon to early evening and the other from late evening to early morning. Three classes of upper-level synoptic pattern seem to be conducive to WSR: i) a "Mongolia front pattern", ii) "northern China front pattern", iii) a "southern front pattern". All of these patterns are accompanied by warm and moist southwesterly flow at low levels. Prior to WSR events, there is usually an upper level trough. According to other studies, such a feature is not usually seen for WSR events in South China.

Accepted for publication in *Monthly Weather Review*. DOI 10.1175/MWR-D-19-0038.1.

1. Introduction

Weather occurring well ahead of a surface cold front is typically described as "pre-frontal" or "warm sector" weather (Omoto 1965; Nozumi and Arakawa 1968). Omoto (1965) indicated that in the United States, to the east of the Rocky Mountains, extensive precipitation zones occur frequently in the warm sectors of cyclones. The lifting mechanism causing the rainfall has been shown to often derive from synoptic-scale disturbances aloft rather than local forcing near the ground. Boustead et al. (2013) also found that significant tornado outbreaks in warm sectors tend to be driven more by synoptic-scale weather systems at upper levels. If the low level environment is favorable, with an ample supply of moisture and convective available potential energy (CAPE), the development of absolute vorticity upstream of the tornadogenesis location can relate to an upper-level jet streak and a negatively tilted mid-level trough. In South China Warm-Sector Rainfall (WSR) occurs frequently during late spring (Huang et al. 1986; Ding 1994), and can deliver extreme rainfall rates and totals. In recent years, greater efforts have been made to study WSR and the related convective initiation in South China by field experiments, numerical simulations and case studies (Zhang et al. 2011; He et al. 2016; Liu et al. 2016; Wu and Luo 2016; Luo et al. 2017; Zhong and Chen 2017).

In contrast, WSR in North China - defined in this study to be within the red rectangle on Fig. 1 - had not generated as much attention until the extreme rainfall event in Beijing on 21 July 2012 (Chen et al. 2012; Zhang et al. 2013; Zhong et al. 2015). Although WSR events in North China are not as frequent as those in South China, more

Accepted for publication in *Monthly Weather Review*. DOI 10.1175/MWR-D-19-0038.1.

and more heavy rainfall cases are reported to be in the WSR class (Xu et al. 2014; Chen et al. 2018; Sun et al. 2018). The intensity, location and timing of such events are currently difficult for operational Numerical Weather Prediction (NWP) models and human forecasters to predict accurately (Zhang et al. 2013; Luo et al. 2017).

Huang et al. (1986) was the first observational study to examine WSR in China. They defined this to be a significant rainfall event that occurs in the warm region 200 km or more ahead of a surface cold front. Some events had no synoptic frontal boundaries within the broader vicinity. According to Huang et al. (1986), meteorologists subjectively characterize WSR events by examining the location of precipitation relative to a surface (or low-level) cold front, or other weather systems (Chen et al. 2012; Wang et al. 2018). Regarding the extreme rainfall event in Beijing on 21 July 2012, the WSR classifications vary greatly from paper to paper. For example, Chen et al. (2012) considered rainfall between 10:00 and 16:00 LST (UTC/GMT +8 hours) to be WSR, whilst Zhong et al. (2015) classified heavy rainfall in the early afternoon (13:00-14:00 LST) as WSR. Sun et al. (2013), on the other hand, divided the rainfall into a pre-frontal stage (10:00-20:00 LST) and a frontal stage (20:00-02:00LST). Increasingly, objective methods have been developed to better characterize the synoptic climatology, identifying weather systems that are associated with severe weather (Jenkner et al. 2009; Meng et al. 2013; He et al. 2017; Huang et al. 2017; Haberlie and Ashley 2018).

Studies of rainfall characteristics, background circulation, mesoscale processes and the underlying physical drivers of WSR in South China have recently been reviewed by

Accepted for publication in *Monthly Weather Review*. DOI 10.1175/MWR-D-19-0038.1.

He et al. (2016). They found that most rainfall events in late spring over South China exhibit characteristics of WSR, whilst the maximum rainfall location is closely related to specific topography. The synoptic patterns for such events can be classified in three categories: i) recirculation of cold air, ii) presence of an upper level trough, and iii) a strong southwesterly monsoon flow. They also demonstrated that boundary layer cold air, and/or topography and/or a thermally driven circulation due to local land/sea contrast may be the main triggering mechanisms for warm sector convective systems in South China. Wu and Luo (2016) recently found that mesoscale boundaries (of low-level convergence) between the convectively generated cold outflow and the southwesterly monsoon flow might provide another triggering mechanism.

For the North China WSR-induced extreme rainfall event of 21 July 2012 in Beijing, it was found that the westward extension of the subtropical high over the western North Pacific and a developing strong low-level jet transporting abundant moisture and energy to the Beijing area together built a favorable environment for torrential rain (Zhao et al. 2013). Yu and Meng (2016) showed that the strength and location of a mid-level trough and a low-level depression were vital factors for the determination of precipitation distribution and intensity. Zhang et al. (2013) and Zhong et al. (2015) indicated that WSR was mostly generated by convective cells triggered by low-level warm and moist southeasterly flows impinging on local topography. .

The current study seeks to develop an objective method to identify WSR, and to examine the WSR-related rainfall climatology and circulation patterns over North China

Accepted for publication in *Monthly Weather Review*. DOI 10.1175/MWR-D-19-0038.1.

through object-oriented composite analysis of all WSR events during the warm seasons (June to September) of 2012 to 2017. The remainder of the paper is organized as follows. Section 2 describes the data and methodology. The 6-year summary statistics of the WSR-related rainstorms are described in section 3. Section 4 presents the synoptic flow patterns present during warm sector rainfall. Finally, a summary is given in section 5.

2. Data and methodology

2.1. Precipitation and reanalysis data

In this study, North China is the box bounded by 110 and 120°E and 34 and 43°N (Fig. 1). The terrain over North China is complex with the Taihangshan and Yanshan Mountain Ranges in the north and west respectively, and the Bohai Sea in the east. Strong rainfall events mainly occur from June to September in North China. The WSR-related rainstorms during these warm-season months from 2012 to 2017 are studied. The rainfall data used herein is a regional gridded dataset, that covers the domain and beyond, and which has a 1-hour temporal resolution and a 0.1 degree spatial resolution. It is provided by China's National Meteorological information Center (http://data.cma.cn/data/detail/dataCode/SEVP_CLI_CHN_MERGE_CMP_PRE_HOUR_GRID_0.10/) and is based on optimal interpolation methods. The inputs consist of reports from 30,000 automatic weather stations in China and a global satellite-based rainfall product called CMORPH developed by NOAA (Pan et al. 2012). There is about 0.01% to 0.05% missing data during the entire study period; we ensured that our analysis

Accepted for publication in *Monthly Weather Review*. DOI 10.1175/MWR-D-19-0038.1.

of WSR-related rainstorms skipped the related dates/times.

The ERA-Interim reanalysis dataset (Simmons et al. 2007) from ECMWF, with a time resolution of 6-hour and a spatial resolution of 0.75X0.75 degrees (http://apps.ecmwf.int/datasets/data/interim-full-daily/levtype=sfc/) is used to analyze the environmental conditions surrounding WSR events in this study. The variables used include direct model output of temperature, geopotential height, relative humidity, specific humidity, precipitable water vapor and CAPE. In ERA-Interim CAPE is calculated by considering parcels of air departing at different model levels below 350hPa. All the ERA-Interim variables used here were available at 6-hour intervals, except for CAPE which was available every 12 hours.

2.2. Identification of WSR

Based on research into WSR in South China (Huang et al. 1986), in which WSR is found in the warm sector, typically 200 km or more from the surface front, a multi-step objective identification method of WSR is developed for our study. The schematic in Figure 2 illustrates the process.

2.2.1 Automatic detection of the low-level synoptic front

1) Renard and Clarke (1965) were the first to objectively locate the front line using a thermodynamic definition. Hewson (1998) later developed a front identification tool to automatically plot atmospheric fronts objectively based on this method. The underpinning

Accepted for publication in *Monthly Weather Review*. DOI 10.1175/MWR-D-19-0038.1.

idea here is that one wants to automatically draw a line, on a low-level pseudo horizontal surface, which follows the warm air boundary of a band of enhanced thermal gradient (Renard and Clark, 1965). Jenkner et al. (2009) adopted and adapted existing algorithms to detect low-level fronts from high-resolution model output over complex terrain. One component of that detection method is heavy smoothing of the input fields. The north and west of North China domain and many adjacent regions are characterized by complex topography. So for simplicity, and considering our overall aims, the present study adopted the algorithms of Jenkner et al. (2009), but with the threshold criteria for each parameter being tuned for the North China region, based in part on operational practice in China Details are outlined below:

1) Choice of variable and pseudo-horizontal level

There are several thermodynamic variables that can be used to define a low-level front (e.g. temperature, potential temperature, equivalent potential temperature). During the summer season in China, temperature gradients between different air masses are often weak. However, a sharp gradient of specific humidity and (therefore) equivalent potential temperature can often be identified (Ninomiya 1984). Therefore, the equivalent potential temperature (θ_e) is used in the present study as the thermal parameter τ.

The formula of θ_e follows (Bolton 1980):

$$\theta_e = T_k \left(\frac{1000}{p}\right)^{0.2854(1-0.28\times10^{-3}r)} \times \exp\left[\left(\frac{3.376}{T_L} - 0.00254\right) \times r(1+0.81\times10^{-3}r)\right] \quad (1)$$

where $T_k, p,$ and r are the absolute temperature, pressure and mixing ratio at the initial level, respectively. T_L is the absolute temperature at the lifting condensation level. In

Accepted for publication in *Monthly Weather Review*. DOI 10.1175/MWR-D-19-0038.1.

order to minimize the potential impacts of interactions between the boundary layer and synoptic fronts aloft, the 850-hPa level, which is near the ground over the western and northern parts of North China and upstream regions, was chosen for the front detection.

2) Smoothing of the initial data

Ordinarily, equivalent potential temperature is not smooth enough for the computation of masking conditions and the locating function, which represent higher order derivatives of τ. By using a simple diffusive smoothing filter (Eqn. 2), equivalent potential temperature and zonal and meridional wind components are preprocessed to eliminate noise. Where n is the filter times and set equal to 3. A much higher value as used by Jenkner et al. (2009) was not needed here because ERA-Interim is much lower resolution than Jenkner's model.

$$\tau_{i,j}^{n} = \frac{1}{2}\tau_{i,j}^{n-1} + \frac{1}{8}(\tau_{i+1,j}^{n-1} + \tau_{i-1,j}^{n-1} + \tau_{i,j+1}^{n-1} + \tau_{i,j-1}^{n-1}) \qquad \mathrm{n} = 1, \ldots, n_f \qquad (2)$$

Fig. 3a provides an example of these pre-processed fields.

3) Detection of front location

A first order horizontal derivative of θ_e (Eqn. 3) is calculated to define the contiguous area that has at least the minimum front strength *K*.

$$|\nabla\theta_e| > K \qquad (3)$$

This threshold is set to 4 K/100 km in this study based on a comparison between manual and objective frontal analyses for typical cases. The front strength is slightly weaker than that used by Jenkner et al. (2009). On the example in Fig. 3b the masked

Accepted for publication in *Monthly Weather Review*. DOI 10.1175/MWR-D-19-0038.1.

areas where K is larger than 4 K/100km are outlined by black contours.

Equation (4) is the formula for calculating the thermal front parameter (TFP); it denotes a second-order horizontal derivative of θ_e.

$$\mathrm{TFP} = -\nabla|\nabla\theta_e| \cdot \frac{\nabla\theta_e}{|\nabla\theta_e|} = 0 \quad (4)$$

$$\nabla \cdot \nabla|\nabla\theta_e| < 0 \quad (5)$$

Initially the front location is defined to be the zero-value contour line of TFP, which coincides with the maximum of the gradient of θ_e. In the terminology of Hewson (1998) this denotes the middle of the "frontal zone". Ordinarily, for forecasters, one would want to identify the line of the TFP maximum, to show the actual front, along the warm air side of the baroclinic zone, which will coincide better with other parameters such as pressure troughs, but for our purposes, where the focus is well away from the front, we do not require that level of specificity. In the example of Fig. 3b the zero line of TFP is marked by green contours, and then Fig. 3c clearly shows how the fronts align with the middle of baroclinic zones.

Note that sometimes a localized minimum gradient of θ_e may be embedded within broad baroclinic zones, due to some discontinuous variation of θ_e. So finally the TFP zero contours are also masked by Equation (5) to ensure that identified fronts coincide with gradient maxima.

The front type is also identified by estimating frontal displacement with time. The direction of movement (Eqn. 6) is by definition perpendicular to a front, and frontal

Accepted for publication in *Monthly Weather Review*. DOI 10.1175/MWR-D-19-0038.1.

velocity can be approximated as follows using the gradient of TFP:

$$\mathbf{V}_f = \boldsymbol{V} \cdot \frac{\nabla(\mathrm{TFP})}{|\nabla(\mathrm{TFP})|} \qquad (6)$$

where $\boldsymbol{V}$ is the horizontal wind vector (at 850hPa). $\mathbf{V}_f$ is positive for a cold front and negative for a warm front while $\mathbf{V}_f = 0$ broadly indicates a stationary front. In the example in Fig. 3c, the front types are mostly well-defined.

4) Distinguishing a synoptic front

Since very localized frontal boundaries usually play a lesser role in regional rainfall, only synoptic fronts are considered for WSR in this study. Here only fronts which are longer than 10 degrees on latitude/longitude grids (about 700 to 1000 km in the study region) are retained as synoptic fronts. Others are deleted. The fronts are detected every 6 hours during the study period. In the Fig. 3 example, note how both the identified fronts extend across a considerable distance.

2.2.2 Objective identification of mesoscale rainstorms

A "mesoscale convective system" is defined as "a cloud system that occurs in connection with an ensemble of thunderstorms and produces a continuous precipitation area of the order of 100km or more in horizontal extent in at least one direction" (American Meteorological Society, 2019). In this study, a mesoscale rainstorm is defined as a continuous rainfall area (CRA), whose attributes, such as intensity and size (in gridded 1-h rainfall totals), are given in Table 1. In the classifications of Li et al. (1998),

Accepted for publication in *Monthly Weather Review*. DOI 10.1175/MWR-D-19-0038.1.

who investigated hourly rainfall intensity over China, our mesoscale rainstorm definition would correspond to a “strong convective rainfall event”. Here our CRA identification method concurs with the proposals of Ebert and McBride (2000); we use our gridded rainfall dataset to estimate areal coverage, centroid, maximum rainfall, etc., for any identified mesoscale rainstorm. All mesoscale rainstorms for each hour during the period from June to September 2012 to 2017 are identified and archived. In the example on Fig. 4, four such rainstorms are identified at 14:00 LST July 21 2012.

2.2.3 Automatic detection of a WSR-related rainstorm

Based on the WSR definition proposed by Huang et al. (1986), the influence area of frontal rainfall is deemed to extend up to 200 km away from the front itself. We identify these limits, as illustrated on Figure 3d. Then any mesoscale rainstorm whose centroid lies outside of the front’s influence area (shaded) is assigned to be a WSR-related rainstorm.

For example, Figure 5 shows the identified fronts (at 8:00 LST) and mesoscale rainstorms (at 13:00 LST) from July 20-31 2012. Two main synoptic frontal systems are detected moving erratically from Inner Mongolia southwards to east China during this period. About 9 mesoscale rainstorms are identified; these are mostly situated near the identified synoptic fronts. Only one of these is assigned to be in the WSR category in North China, on panel (b) near the border between Hebei and Beijing. This is in fact the first stage (13:00 to 14:00 LST) of the extreme rainfall event of 21 July 2012 examined in

Accepted for publication in *Monthly Weather Review*. DOI 10.1175/MWR-D-19-0038.1.

Zhong et al. (2015). It is situated in the tongue of high equivalent potential temperature ahead of the identified cold front. This event illustrates well the effectiveness of this automatic method for detecting WSR. And there are naturally some clear benefits relative to manual analysis, such as reduced manpower and consistency of approach. Based on our method described above, a total of 768 WSR rainstorms were automatically identified during the warm-season months of the 6-year study period. In the next sub-section we analyze their morphology and temporal and spatial distributions.

Three experiments are made to discuss the uncertainty of the identified WSR events due to the different time intervals of rainfall and circulation data. The comparative experiments and the strategy used in present study are shown in Table 2. Indeed, it shows some variance in the number of shared WSR events, with a maximum bias of 92 and minimum bias of 38, comparing to the identification strategy used. The errors of the WSR events are possibly related to the different stages (such as formation, movement, dissipation) of the life-cycle of a surface front. Take the Fig.5b as an example, a WSR event at 13:00 LST 21 July 2012 in North China is identified when the front at 8:00 LST is used, which is consistent with the definition of Zhong et al. (2015). But the same WSR event will not be identified when the front at 14:00 LST, which is located over north of North China, is employed. According to the 6-hour interval circulation data, the stage and location of the front during the period of 09-13:00 LST are not sure. For the newly formed or slowly moving front at 14:00 LST, the front at 8:00 LST should be used. However for the fast moving front system, the front at 14:00 LST would be better.

Accepted for publication in *Monthly Weather Review*. DOI 10.1175/MWR-D-19-0038.1.

2.3. Classification of circulation patterns

To further understand the synoptic background of WSR, the circulation patterns associated with various WSR-related rainstorms are subjectively classified into several categories using the 6-hourly reanalysis data. Figure 6 shows the distribution and frequency of identified frontal boundaries for the scenarios when WSR-related rainstorms occur between June and September in the years 2012 to 2017. There seem to be two high frequency centers, one running approximately northeast-southwest through Inner Mongolia, the other situated approximately between the Yangtze-Huai Rivers. The front frequency north of 45°N (Mongolia) is relatively low during this period. Ding and Chan (2005) noted that the synoptic frontal zone tends to experience several northward jumps with the northward progression of the East Asia summer monsoon: the west-east-oriented frontal zone tends to be situated in South China from April to May, firstly shifts to the Yangtze-Huai River Valley in early June, subsequently leaps to North China around mid-July, and typically begins to retreat southward in mid-August.

The frontal boundaries related to WSR-related rainstorm events can be divided into three categories based on the location of the fronts, namely, the Mongolia front (north of 45°N), the northern China front (between 35 and 45N°), and the Yangtze-Huai River front (south of 35°N), which are respectively indicated by grey, blue and red lines in Figure 6a. At any given time, there are eight possible scenarios regarding frontal boundaries identified over East Asia, just one of the above fronts, two or three of them, or none. The frequencies of the eight possible scenarios of fronts when WSR-related

Accepted for publication in *Monthly Weather Review*. DOI 10.1175/MWR-D-19-0038.1.

rainstorm events occur are summarized in Table 3. Scenario (II), only a northern China front, is the most populated category accounting for 29% (83 samples). The three scenarios that include a northern China front and one other (IV, VI, and VII), together account for about 34% (98 samples in total). The scenarios (III and V), in which Yangtze-Huai River fronts are dominant, account for 21% (60 samples in total). The remaining scenarios (I and VIII) account for just 16% of all cases (47 in total).

We next composite the synoptic circulation patterns using the arithmetic mean of 500-hPa geopotential height present during the events in each of the eight scenarios. Since this shows that some scenarios share similar synoptic flow characteristics, we then subjectively merge together some of these eight patterns to arrive at just three. The deciding factors in this process were the location of a 500-hPa trough, the positioning of the West Pacific Subtropical High, and indeed the locations of the frontal zones themselves. The first circulation pattern consists of all events with only a Mongolia front identified (I), which we call the "Mongolia front pattern". The second circulation pattern, which we call the "northern China front pattern", is obtained by combining five scenarios (II, IV, VI, VII), which share a circulation pattern similar to that associated with scenario (II) ("only northern China front") or/and in which northern China fronts are identified . The third circulation pattern is defined by events where Yangtze-Huai River fronts are dominant (III, V). This we label the "southern front pattern". Due to no identified front for scenario VIII, compared with the upper three patterns, the circulation of scenario VIII is not composited with any of them. But it has similar circulation with northern China

Accepted for publication in *Monthly Weather Review*. DOI 10.1175/MWR-D-19-0038.1.

front pattern and not shown here. The dynamic, thermodynamics, and moisture conditions associated with each of these three patterns are composited to analyze the environmental conditions for WSR.

3. **Statistics of WSR-related rainstorms**

WSR-related rainstorm frequency plots (Fig. 7) are generated by counting the total number of cases in a one-degree box, with box assignation dependent on where the rainstorm centroid was located. The rainstorms mainly occur on the plains over the central-eastern part of North China with two peak frequencies, one at somewhat higher altitudes just south of the Yanshan Mountain Range, and the other near the junction of the Henan, Shandong and Jiangsu provinces (Fig. 7a). The annual mean rainfall of North China (not shown) is also characterized by a gradual decrease from southeast to northwest with two maxima, one in northeast part of Hebei province, and the other in the southeast region of North China. He and Zhang (2010) indicated that on average, rainfall amount over the North China plain is higher than it is over the higher terrain north of this. They attributed the rainfall distribution to be at least partially the impacts of regional mountain-plains solenoid on rainfall diurnal variations. A similar spatial distribution is found here for the WSR rainstorms. Meanwhile, the location of the peak frequency of WSR rainstorm near to the junction of the three provinces is consistent with the peak frequency of occurrence of squall lines in North China (Meng et al. 2013). That may provide a mesoscale “explanation” for this being a focal point of WSR rainstorm events.

Accepted for publication in *Monthly Weather Review*. DOI 10.1175/MWR-D-19-0038.1.

Compared to the front line frequency distribution (Fig. 6b), WSR rainstorm events are mainly located southeast ("downstream") of the northern China front and northwest ("upstream") of the Yangtze-Huai River front.

Figure 7b-d show intra-seasonal variations in the spatial distribution of WSR rainstorm events. The rainstorm events can occur from June to September. However, whilst climatologically the main rain belt stays in Central China from Mid-June to Mid-July, there is still a relatively high frequency over the south and east of North China region, with a maximum frequency over the boundaries between Shandong and Henan (Fig. 7b). Between mid-July and mid-August, the WSR rainstorm event distribution (Fig. 7c) resembles the total warm season distribution (Fig. 7a) and is similarly much more amplified than in the other two periods. When the main rain belt jumps to North China, another frequency peak appears over the northeast of North China (Figure 7c). And when the rain belt retreats southward from mid-August to mid-September, the frequency of WSR rainstorm events decreases significantly, although the northern focal point within the North China region persists (Figure 7d).

The WSR-attributable rainfall fraction is derived by dividing the total rainfall amount from WSR rainstorm events by total rainfall from of all identified mesoscale rainstorms over North China during the summer-time analysis period. Although the WSR fraction is about 5 to 10% over most of the plains in North China, which is not as much as it is in South China during the late spring season (He et al. 2016), locally WSR events account for as much as 15% to 25% of total rainfall. This is seen particularly in areas that

Accepted for publication in *Monthly Weather Review*. DOI 10.1175/MWR-D-19-0038.1.

are somewhat more topographically complex, such as the north-central part of Tianjin, the northeast of Hebei province, the northwest of Henan province, and central part of Shandong province (Fig. 8a). The WSR over the above regions may be closely associated with mesoscale processes and local factors, such as mountain-associated lifting and land–sea contrasts (Wu and Luo 2016). In respect of whether a rainstorm event will be WSR-related, there is about 40% chance in each sub-period (Fig. 8b). This is irrespective of whether the main rain belt is situated in North China or not. Yeh and Chen (1998) indicated that about 50% of the rainfall occurred as scattered orographic showers in non-front periods during the Taiwan Area Mesoscale Experiment.

In respect of the morphology of WSR rainstorms, the areas of the identified rainstorm (rainfall amounts >5 mm/hr) (Fig. 9a) and of more extreme conditions (>10 mm/hr) (Fig. 9b) are respectively about 5000 to 20000 km^2 and 2500 to 10000 km^2, with means of 12000 km^2 and 5900 km^2. The maximum rainfall of WSR rainstorm events is mostly about 20 to 40 mm/hr, with a mean value of 35mm/hr, and an extreme hourly total of 89 mm (Fig. 9c). For the diurnal variation, there are two peaks, one from afternoon to early evening (14:00 to 22:00 LST) and the other from midnight to early morning (1:00 to 7:00 LST). The first peak has a slightly larger, which may indicate that solar radiation plays an important triggering role. Recent papers revealed that nocturnal precipitation in the warm season over North China is often associated with the initiation and movement of convective systems triggered over the eastern edges of plateaus in the afternoon, which subsequently propagate to the plain area overnight (He and Zhang 2010; Bao and Zhang

Accepted for publication in *Monthly Weather Review*. DOI 10.1175/MWR-D-19-0038.1.

2013; Yuan et al. 2014). The mountain-plains solenoid circulation, a low-level southwesterly nocturnal jet and cold pool dynamics are likely to be jointly responsible for nighttime precipitation enhancement (He and Zhang 2010; Bao and Zhang 2013).

4. Composite analysis of the synoptic flow patterns of WSR

The large-scale circulation of all WSR-related rainstorms was further classified into three synoptic patterns, named the Mongolia front pattern, the northern China front pattern, and the southern front pattern. Fig. 10 shows the composite 500hPa geopotential height, 850hPa wind vector and identified average fronts as well as centroids of all WSR-related rainstorms for each. All three patterns are characterized by the presence of a synoptic or short-wave trough, with the influence also of a subtropical high over central eastern China and the northwest Pacific. The northern China front pattern, with a trough in west of North China and a subtropical high to the southeast, accounts for 69.6% of the total. The northern China front pattern is one of the typical synoptic types that deliver heavy rainfall in North China (Book Writing Team of North China Heavy rainfall, 1992). 20.8% of cases belong to the southern front pattern, which has a trough over North China and the front over Yangtze-Huai River valley (Fig. 10c). The Mongolian front pattern, which is characterized by a short-wave on the periphery of the subtropical high, is relatively uncommon, featuring only 6.6% of the time (Fig. 10a).

For the Mongolian front pattern (Fig. 10a), a continental high pressure center controls the north part of East Asia with the short wave trough over the Huang-Huai

Accepted for publication in *Monthly Weather Review*. DOI 10.1175/MWR-D-19-0038.1.

inter-river region and the subtropical high along the east coast of China. A strong southwesterly current flowing from South China into North China with convergence implied over the eastern part of North China, which may help with forcing ascent. Most of the identified WSR-related rainstorms are located over the southern part of North China. All are situated at cyclonic curvature or left side of the strong southerly flow.

For the northern China front pattern (Fig. 10b), the mean cold front is mainly situated to the Northwest China (upstream) of North China. The trough is over western North China, while the subtropical high is relatively far south, with its northern edge at the south of the Huang-Huai inter-river region. North China is controlled by the southwesterly flow, as was the case for the Mongolian front pattern, but with the leading edge of strong southwesterlies over the south of North China. The identified WSR-related rainstorms lie on the leading edge of or within the strong southwesterly. Nearly three quarters of the rainstorms in North China occurred under this synoptic pattern. The extreme event in Beijing on July 21 2012 had a similar circulation pattern (Sun et al., 2013). The coexistence of the subtropical high and the upper-level trough will lead to the development and enhancement of southerly flow, as was identified by Zhong et al. (2015) for the July 21 2012 extreme event in Beijing. The southerly not only transports abundant water vapor and convective energy to North China, but also supports the development of convective systems by convergence or shear in the strong southerly flow, as well as by lifting forced by the Taihang Mountains.

With respect to southern front pattern (Figure 10c), the front zone is relatively far

Accepted for publication in *Monthly Weather Review*. DOI 10.1175/MWR-D-19-0038.1.

south and the front boundary mainly affects the Yangtze River Basin in China. A northeast - southwest oriented trough extends from Inner Mongolia to west of Huanghuai valley with the main body of the subtropical high situated in the northwestern Pacific. North China is under the control of the trough. All identified WSR-related rainstorms lie beneath the bottom of the trough or west of the trough ("post-trough"). Compared to the low level flows of the Mongolian front pattern and the northern China front pattern, the southerly at low level is ahead of the trough, and disconnected from the southerly current along northwest of the subtropical high. This has been caused by the southeastward withdrawal of the subtropical high. The high CAPE and PW is separated from the main pool of tropical moisture over and south of the Mei-Yu region. The shear line between northwesterly and southwesterly at 850hPa lies slightly more westward compared to the upper level trough at 500hPa. It indicates that it is a negatively tilted synoptic system. This circulation pattern resembles that of the decaying upper-level cold vortex (Gao and He, 2013), although there is no closed upper level circulation identified on the composited plot. At the decaying stage of cold vortex, the low level cold northerly flow obviously decreases and southerly winds prevail under and ahead of the trough line (Liu et al., 2012). Height disturbances (i.e. short wave) behind of the trough frequently develop, which may lead to convective weather. Gao and He (2013) indicated that heavy convective precipitation can occur at the decaying stage of cold vortex in North China.

Past studies have pointed out that moisture at low levels and CAPE are important for the development of WSR (Zhong et al. 2015; Wu and Luo 2016; Luo et al. 2017). The

Accepted for publication in *Monthly Weather Review*. DOI 10.1175/MWR-D-19-0038.1.

composited equivalent potential temperature is characterized by a high-value tongue extending to North China with the identified WSR-related rainstorms lying within that tongue (not shown). Fig. 11 shows the composited precipitable water vapor (PWAT) as contours and CAPE with shading. Similar to the distribution of equivalent potential temperature, a tongue of high PWAT extends into North China for all three patterns. The average PWAT is about 50mm for the Mongolian and northern China front patterns, due to the warm, moist flow on the northwest periphery of the subtropical high. The PWAT for the southern front pattern is slightly less, with a mean value of about 40 mm. In respect of the convective instability, the mean CAPE for the Mongolian front pattern is about 500 to 1000J/kg with the identified WSR-related rainstorms lying on the northwestern periphery of the maximum. However, the maxima of CAPE of the China continent controls North China for the northern China front pattern, with a mean larger than 1000 J/kg. There is a secondary, more isolated maximum of CAPE over North China for the southern front pattern, with the average value 500 to 800J/kg. Clearly, for the southern front pattern, moisture pooling and instability energy occur in conjunction with the trough, and highlights the importance of cold temperatures aloft and decreased stability with the trough. These ingredients are a bit different than the other two patterns that have a direct "tap" to the tropical moisture to the south.

As stated by Luo et al. (2017), warm sector heavy rainfall is not well forecasted either by the operational NWP models or by human weather forecasters. So the identification of favorable environment conditions, from NWP forecast fields, can assist

Accepted for publication in *Monthly Weather Review*. DOI 10.1175/MWR-D-19-0038.1.

in discriminating the potential for WSR. Conditions present before WSR should also be valuable to analyze possible outcomes. The circulations 6 to 24-hour ahead of WSR-related rainstorms have also been composited here. In order to exclude the influence of persistent WSR-related scenarios, only circulations at the start of these events have been used.

Figure 12 shows the composited 500hPa geopotential height and 850hPa wind 6 hours ahead of the identified WSR-related rainstorms. For the Mongolian front pattern, the short wave was present 6 hours ahead of the WSR rainstorms (Figure 12a), and even 12 and18 hours ahead (not shown). For the northern China front pattern, there is a weak trough upstream of North China and the subtropical high is a little south of where it is when the rainstorms occur (Figure 12b). A height disturbance begins to develop over central and western Inner Mongolia 6 hours ahead with a relative weaker southerly flow compared to that when WSR rainstorms occurs for the southern front pattern (Figure 12c). Compared to Fig.10, the southerly winds at low levels and the upper level troughs seems to get stronger from 6 hours ahead to just the time when the rainstorms occur for all three patterns.

The height differences at 500 hPa among the three patterns are calculated. The similar positive differences of 500 hPa heights between Mongolia front and the other two patterns are statistically significant over eastern Mongolia to Northeast China (Figure 13 a and b), which is caused by the discrepancy of broad high for Mongolia front pattern and troughs for the other two patterns. Between northern China front and the southern one,

Accepted for publication in *Monthly Weather Review*. DOI 10.1175/MWR-D-19-0038.1.

significant differences of 500 hPa height are found over North China and Northwestern Pacific Ocean due to the distinct locations of their troughs and subtropical highs (Figure 13c).

The circulation of each pattern is characterized by the developing of the short wave trough or trough at upper levels. This is different from the upper-level synoptic pattern of WSR in South China, most of which has no prominent synoptic-scale lifting (Wu and Luo 2016). As a human forecaster, identifying pre-cursor disturbances, such as upper-level synoptic or short-wave troughs, can be useful for highlighting the potential for the development of WSR, alongside an analysis of the boundary triggering mechanisms in North China. On the one hand, the upper level trough may provide a dynamic explanation for the development of mesoscale systems at the lower level. On the other hand, the trough may bring cold and dry air over the warm moist flow at the lower levels which will be helpful to generate potential convective instability.

5. Concluding remarks

Using gridded rainfall data and ERA Interim reanalysis data, this work has investigated the general features of WSR in North China during the months June to September in the years 2012 to 2017. It may provide valuable background information for human forecasters in warning of the potential occurrence of WSR.

WSR is defined to be located outside of a frontal influence area, requiring a separation of > 200 km from either side of the front. One might argue that the cold side of

Accepted for publication in *Monthly Weather Review*. DOI 10.1175/MWR-D-19-0038.1.

a front is not the warm sector; however, the region of study, in the summer season, ordinarily lies in extensive ‘warm sector’ conditions well south of a primary cold front typically found north of China. More localized fronts can be found within this broad warm sector, and the rainbands connected to these are directly excluded with this double-sided condition. Based on our WSR definition, an objective identification of WSR was first developed. There are three steps in this procedure, including the detection of fronts and their areas of influence, mesoscale rainstorm identification, and WSR discrimination. This method helps meteorologists to select the WSR cases with higher efficiency in a way that is consistent for climatological analysis.

This survey identified 768 WSR rainstorm events in total during the warm-season months of a 6-year period，which are mainly located over the plains of North China, with two maximum frequency regions, one to the south of the Yanshan Mountain Range and the other over the junction of Henan, Shandong and Jiangsu provinces. The two peak areas may be related to topographic effects and frequently observed squall lines. WSR can occur in North China from June to September, with a peak in Mid-July to Mid-August. The higher WSR frequency moves northwards across North China between mid-June and mid-August with a clear reduction in frequencies after mid-August. This is all associated with the natural progression of the East Asian summer monsoon. Although WSR does not occur very often in North China it can still account for 15 to 25% of total rainfall during warm season over some smaller-scale topographically complex regions. And about 40% of identified mesoscale rainstorms are WSR-related in North China

Accepted for publication in *Monthly Weather Review*. DOI 10.1175/MWR-D-19-0038.1.

during the warm season.

The areal coverage of WSR-related rainstorms with rainfall intensity larger than 10 mm/hr are mostly 2500 to 10000 km^2 with mean areal coverage of 5900 km^2. The maximum rainfall of the rainstorms is mostly 20 to 40 mm/hr with an average maximum 1h rainfall of 35mm and extreme maximum of 89mm. There are diurnal peaks of WSR, one from afternoon to early evening (14:00 to 22:00 LST) and the other during nighttime (1:00 to 7:00 LST), respectively, which has a similar diurnal variation to convective rainfall in general across North China. The nighttime peak may be associated with the mountain-plains solenoid circulation, a low level southwesterly and cold pool dynamics of MCS.

Based on the location of identified fronts of WSR-related rainstorms their circulations are classified into three synoptic patterns: i) the Mongolian front pattern with a short-wave trough in the south of north China along the periphery of the subtropical high, ii) the northern China front pattern with a trough in the west of north China and a subtropical high in the south and iii) the southern front pattern with a negative tilted trough over North China, all of which are accompanied by warm and moist southwesterly flow at low levels. The most frequent pattern is North China front pattern, which accounts for 69.6% of the total WSR events. The moisture and convective instability energy of north front pattern and North China front pattern have similar features with an average PWAT of 50mm and CAPE of about 1000 J/kg. The water vapor and energy of south front pattern are a little bit less with the average PWAT of 40 mm and CAPE of 500

Accepted for publication in *Monthly Weather Review*. DOI 10.1175/MWR-D-19-0038.1.

to 800J/kg. A trough or short wave trough for all three pattern are found at and at least 6h ahead of the time when WSR rainstorms occur. The patterns are generally different from what is seen for WSR in South China. Analyzing disturbances at upper levels as well as the favorable low-level environmental conditions would assist human forecasters in discriminating the potential for WSR.

This present work has only summarized the basic characteristic and circulation patterns of WSR in North China. The precise mechanism(s) of the heavy rainfall over the warm sector and its predictability need to be further investigated in the future. First of all, the background environment only provides the necessary conditions, but whether the WSR will develop or not still needs to be looked into via systematic examinations of both WSR and non-WSR cases. In particular, we also need more research on the initiation and maintenance mechanisms, or otherwise, for convective systems related to WSR. In addition, the performance of NWP models should be further examined, by assessing both operational and alternative NWP products, and by conducting cloud-resolving numerical simulations of both WSR and non-WSR cases.

Acknowledgements: We are grateful to Dongbin Zhang for providing the gridded rainfall dataset and for comments from two anonymous reviewers. This research was sponsored by project supported by the National Key Research and Development Program of China (Grant No. 2018YFC1507703) and National Key Technologies R & D Program of China (Grant No. 2015BAC03B00). Partial support is provided by the US NSF grant

Accepted for publication in *Monthly Weather Review*. DOI 10.1175/MWR-D-19-0038.1.

AGS-1712290.

References

American Meteorological Society, cited 2019: Mesoscale convective system. Glossary of Meteorology. [Available online at http://glossary.ametsoc.org/wiki/Mesoscale_convective_system]

Bao, X., and F. Zhang, 2013: Impacts of the mountain–plains solenoid and cold pool dynamics on the diurnal variation of warm-season precipitation over northern China. *Atmos. Chem. Phys.*, **13,** 6965-6982.

Bolton, D., 1980: The Computation of Equivalent Potential Temperature. *Monthly Weather Review*, **108,** 1046-1053.

Book Writing Team of North China Heavy rainfall,1992: Heavy rainfall in North China.Beijing,China Meteorological Press, 182PP.

Boustead, J. M., B. E. Mayes, W. Gargan, J. L. Leighton, G. Phillips, and P. N. Schumacher, 2013: Discriminating Environmental Conditions for Significant Warm Sector and Boundary Tornadoes in Parts of the Great Plains. *Weather and Forecasting*, **28,** 1498-1523.

Chen, Y., and Coauthors, 2012: Analysis and thinking on the extremes of the 21 July 2012 torrential rian in Beijing Part I: Observation and Thinking. *Meteorological Monthly*, **38,** 1255-1266.

Chen, Y., and Coauthors, 2018: Analysis of a forecast failure case of warm sector

Accepted for publication in *Monthly Weather Review*. DOI 10.1175/MWR-D-19-0038.1.

torrential rainfall in North China. Meteorological Monthly. *Meteorological Monthly*, **44,** 15-25.

Ding, Y., 1994: *Monsoons over China.* Kluwer Academic Publishers,Dordrecht,Netherlands, 419 pp.

Ding, Y., and J. C. L. Chan, 2005: The East Asian summer monsoon: an overview. *Meteorology and Atmospheric Physics*, **89,** 117-142.

Ebert, E. E., and J. L. McBride, 2000: Verification of precipitation in weather systems: determination of systematic errors. *Journal of Hydrology*, **239,** 179-202.

Gao Y., and L., He. 2013: The Phase Features of a Cold Vortex over North China. *Journal of Applied Meteorological Science*,**24(6)**: 704-713.

Haberlie, A. M., and W. S. Ashley, 2018: A Method for Identifying Midlatitude Mesoscale Convective Systems in Radar Mosaics. Part I: Segmentation and Classification. *Journal of Applied Meteorology and Climatology*, **57,** 1575-1598.

He, H., and F. Zhang, 2010: Diurnal Variations of Warm-Season Precipitation over Northern China. *Monthly Weather Review*, **138,** 1017-1025.

He, L., T. Chen, and Q. Kong, 2016: A review of Studies on prefrontal torrential rain in South China. *Journal of Applied Meteorological Science*, **27(5),** 559-569.

He, Z., Q. Zhang, L. Bai, and Z. Meng, 2017: Characteristics of mesoscale convective systems in central East China and their reliance on atmospheric circulation patterns. *International Journal of Climatology*, **37,** 3276-3290.

Hewson, T. D., 1998: Objective fronts. *Meteorological Applications*, **5,** 37-65.

Accepted for publication in *Monthly Weather Review*. DOI 10.1175/MWR-D-19-0038.1.

Huang, S., Z. Li, and C. Bao, 1986: *Heavy Rainfalls in the pre-rainy season in South China.* Guangdong Science and Technology Press,Guangzhou,China, 230 pp.

Huang, Y., Z. Meng, J. Li, W. Li, L. Bai, M. Zhang, and X. Wang, 2017: Distribution and Variability of Satellite‐Derived Signals of Isolated Convection Initiation Events Over Central Eastern China. *Journal of Geophysical Research: Atmospheres*, **122,** 11,357-311,373.

Jenkner, J., M. Sprenger, I. Schwenk, C. Schwierz, S. Dierer, and D. Leuenberger, 2009: *Detection and climatology of fronts in a high‐resolution model reanalysis over the Alps.* Vol. 17, 1-18 pp.

Li, L., Y.-j. Zhu, and B. Zhao, 1998: Rain rate distributions for China from hourly rain gauge data. *Radio Science*, **33,** 553-564.

Liu, R., J. Sun, J. Wei, and S. Fu, 2016: Classification of persistent heavy rainfall events over South China and associated moisture source analysis. *Journal of Meteorological Research*, **30,** 678-693.

Liu Y., and Coauthors, 2012:A comprehensive analysis of the structure of a northeast China-cold-vortex and its characteristics of evolution. *Acta Meteorologica Sinica*, **70(3)**: 354-370.

Luo, Y., and Coauthors, 2017: The Southern China Monsoon Rainfall Experiment (SCMREX). *Bulletin of the American Meteorological Society*, **98,** 999-1013.

Meng, Z., D. Yan, and Y. Zhang, 2013: General Features of Squall Lines in East China. *Monthly Weather Review*, **141,** 1629-1647.

Accepted for publication in *Monthly Weather Review*. DOI 10.1175/MWR-D-19-0038.1.

Ninomiya, K., 1984: Characteristics of Baiu Front as a Predominant Subtropical Front in the Summer Northern Hemisphere. *Journal of the Meteorological Society of Japan. Ser. II*, **62,** 880-894.

Nozumi, Y., and H. Arakawa, 1968: Prefrontal rain bands located in the warm sector of subtropical cyclones over the ocean. *Journal of Geophysical Research*, **73,** 487-492.

Omoto, Y., 1965: On Pre-Frontal Precipitation Zones in the United States. *Journal of the Meteorological Society of Japan. Ser. II*, **43,** 310-330.

Pan, Y., Y. Shen, J. Yu, and P. Zhao, 2012: Analysis of the combined gauge-satellite hourly precipitation over China based on the OI technique. *Acta Meteorologica Sinica*, **70,** 1381-1389.

Renard, R. J., and L. C. Clarke, 1965: Experiments in numerical objective frontal analysiS. Monthly Weather Review, 93, 547-556.

Simmons, A., S. Uppala, D. Dee, and S. Kobayashi, 2007: ERA-Interim: New ECMWF reanalysis products from 1989 onwards. *ECMWF Newsletter*, ECMWF.

Sun, J., S. Zhao, and S. Fu, 2013: Multi-scale characteristics of record heavy rainfall over Beijing area on July 21, 2012 *Journal of Atmospheric Science*, **37,** 705-718.

Sun, M., X. Wang, L. Hu, H. Chen, and T. Han, 2018: Study on initiation and propagation mechanism of a warm-sector torrential rain in North China. *Meteorological Monthly*, **44,** 1255-1266.

Wang, L., Y. Chen, T. Xiao, S. Li, and L. Ge, 2018: Statistical Analysis of Warm-Sector Rainstorm Characteristics over the Southern of Middle and Lower Reaches of the

Accepted for publication in *Monthly Weather Review*. DOI 10.1175/MWR-D-19-0038.1.

Yangtze River in Summer. *Meteorological Monthly*, **44,** 771-780.

Wu, M., and Y. Luo, 2016: Mesoscale observational analysis of lifting mechanism of a warm-sector convective system producing the maximal daily precipitation in China mainland during pre-summer rainy season of 2015. *Journal of Meteorological Research*, **30,** 719-736.

Xu, J., S. Yang, J. Sun, F. Zhang, and Y. Chen, 2014: Discussion on the formation of a warm sector torrential rain case in North China. . *Meteorological Monthly*, **40,** 1455-1463.

Yeh, H.-C., and Y.-L. Chen, 1998: Characteristics of Rainfall Distributions over Taiwan during the Taiwan Area Mesoscale Experiment (TAMEX). *Journal of Applied Meteorology*, **37,** 1457-1469.

Yu, H., and Z. Meng, 2016: Key synoptic-scale features influencing the high-impact heavy rainfall in Beijing, China, on 21 July 2012. *Tellus A: Dynamic Meteorology and Oceanography*, **68,** 1-15.

Yuan, W., W. Sun, H. Chen, and R. Yu, 2014: Topographic effects on spatiotemporal variations of short-duration rainfall events in warm season of central North China. *Journal of Geophysical Research: Atmospheres*, **119,** 11,223-211,234.

Zhang, D. L., Y. Lin, P. Zhao, X. Yu, S. Wang, H. Kang, and Y. Ding, 2013: The Beijing extreme rainfall of 21 July 2012: "Right results" but for wrong reasons. *Geophysical Research Letters*, **40,** 1426-1431.

Zhang, R., Y. Ni, L. Liu, Y. Luo, and Y. Wang, 2011: South China Heavy Rainfall

Accepted for publication in *Monthly Weather Review*. DOI 10.1175/MWR-D-19-0038.1.

Experiments (SCHeREX). *Journal of the Meteorological Society of Japan. Ser. II*, **89A,** 153-166.

Zhao, Y., Q. Zhang, Y. Du, M. Jiang, and J. Zhang, 2013: Objective analysis of circulation extremes during the 21 July 2012 torrential rain in Beijing. *Acta Meteorologica Sinica*, **27,** 626-635.

Zhong, L., R. Mu, D. Zhang, P. Zhao, Z. Zhang, and N. Wang, 2015: An observational analysis of warm-sector rainfall characteristics associated with the 21 July 2012 Beijing extreme rainfall event. *Journal of Geophysical Research: Atmospheres*, **120,** 3274-3291.

Zhong, S., and Z. Chen, 2017: The Impacts of Atmospheric Moisture Transportation on Warm Sector Torrential Rains over South China. *Atmosphere*, **8,** 1-16.

Accepted for publication in *Monthly Weather Review*. DOI 10.1175/MWR-D-19-0038.1.

Table 1. Attributes defining a “mesoscale rainstorm” in this study (values in mm are 1h rainfall totals from the gridded rainfall analysis)

Definition	1h rainfall total	Heavy rainfall sub-area	Length of heavy rainfall sub-area*	Maximum rainfall
a continuous rainfall area	>= 5mm	>=10mm	>= 100 km in at least one direction	>=20mm

* The length here represents the size of its main axis in any direction, which goes through the mass center of a sub-area.

Accepted for publication in *Monthly Weather Review*. DOI 10.1175/MWR-D-19-0038.1.

Table 2. Information of the WSR identification strategy used in present research (No.0) and the three comparative experiments (No.1-3).

Experiment No.	Time of front	Time of rainfall	No. of WSR events	No. of shared WSR events with No.0
1	T	T to T+5h	761	730
2	T	T-1h to T+4h	764	701
3	T	T-2h to T+3h	767	676
0	T	T+1 to T+6h	768	768

Accepted for publication in *Monthly Weather Review*. DOI 10.1175/MWR-D-19-0038.1.

Table 3. The frequency of eight front-relative scenarios related to WSR rainstorms.

Category	Definition	No. of samples
I	Only Mongolia front	19
II	Only northern China front	83
III	Only Yangtze-Huai River front	35
IV	coexistence of Mongolia front and northern China front	39
V	coexistence of Mongolia front and Yangtze-Huai River front	25
VI	coexistence of northern China front and Yangtze-Huai River front	43
VII	coexistence of Mongolia front, northern China front, and Yangtze-Huai River front	16
VIII	No front	28

Accepted for publication in *Monthly Weather Review*. DOI 10.1175/MWR-D-19-0038.1.

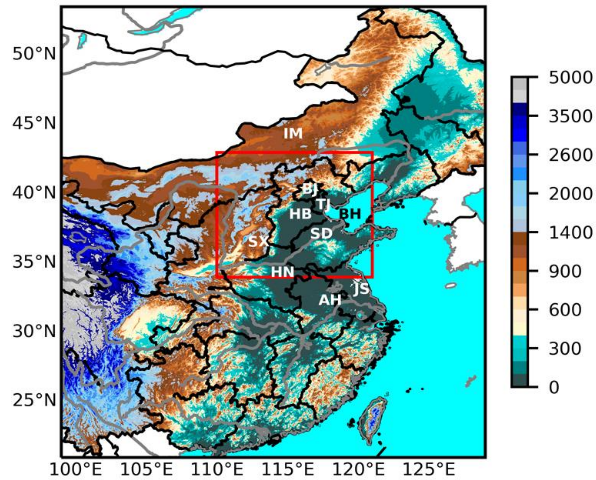

Fig.1 Study domain and the topography over China (shaded, unit: m). The red rectangle represents North China and white text denotes the cities of Beijing (BJ) and Tianjin (TJ), and the provinces of Shanxi (SX), Hebei (HB), Shandong (SD), Inner-Mongolia(IM), Henan(HN), Anhui(AH) ,Jiangsu (JS). Bohai sea (BH) is marked by black text.

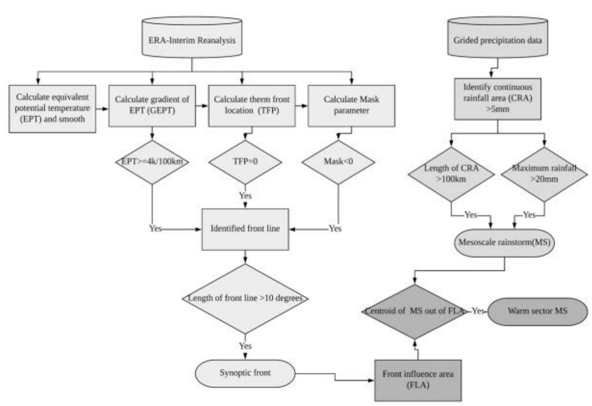

Accepted for publication in *Monthly Weather Review*. DOI 10.1175/MWR-D-19-0038.1.

Fig.2 Flow chart of automatic method used to identify frontal boundaries, mesoscale rainstorms, and warm sector mesoscale rainstorms. Data (cylinders), processes (rectangles), decisions (diamonds) and final solutions (oval) are all presented.

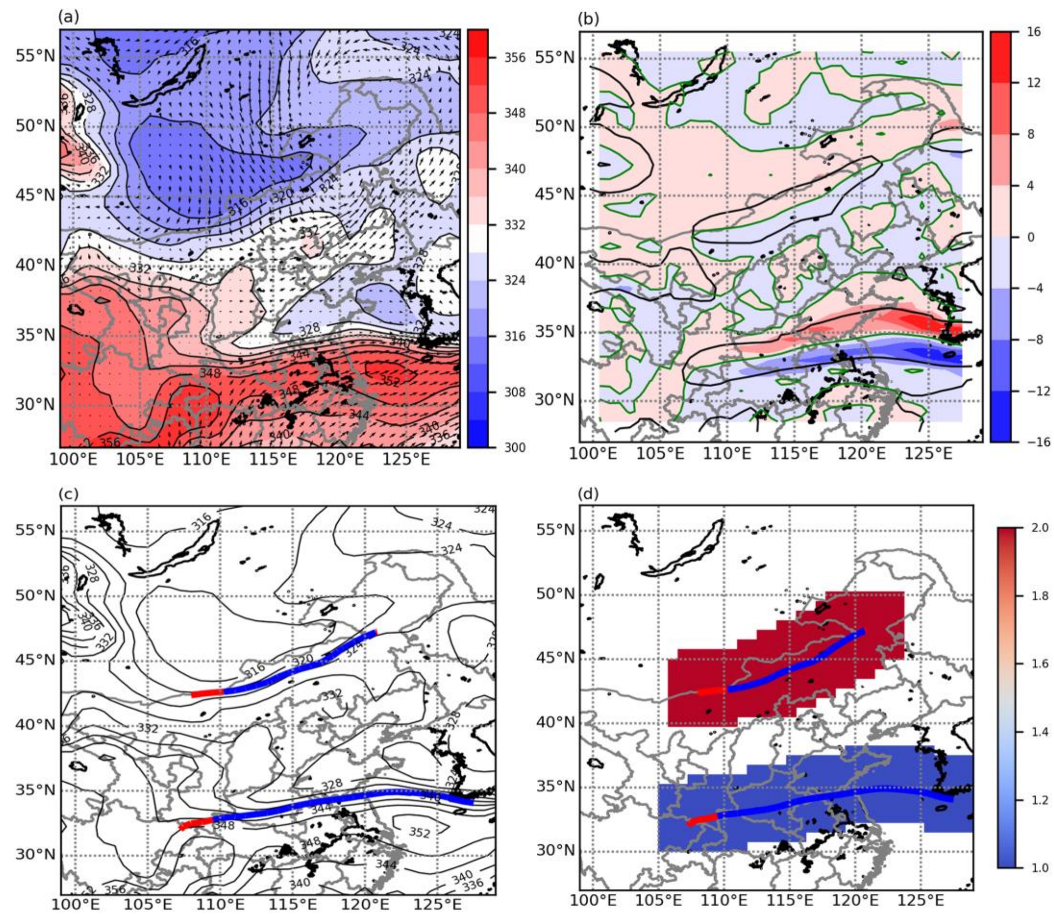

Fig.3 Data for 08:00 LST July 1 2012: (a) Smoothed equivalent potential temperature (K, shaded) and wind vectors at 850hPa, (b) thermal front parameter (shaded) with zero contours (green) and gradient of equivalent potential temperature =4 K/100km (black contours), (c) equivalent potential temperature (black contours) and synoptic front boundaries (blue/red), (d) front boundaries and their areas of influence (shaded).

Accepted for publication in *Monthly Weather Review*. DOI 10.1175/MWR-D-19-0038.1.

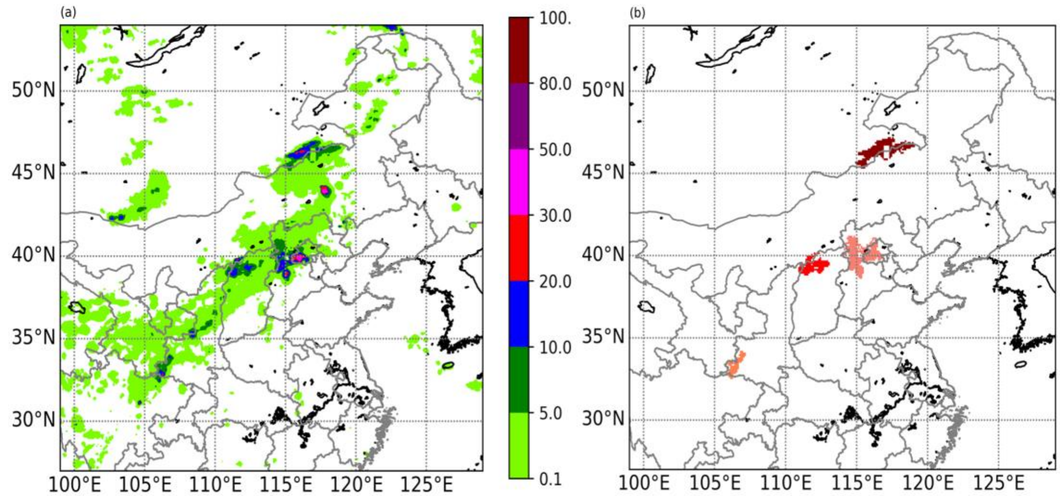

Fig.4 (a) The distribution of 1h rainfall (mm) and (b) identified mesoscale rainstorms for 13:00-14:00 LST 21 July 2012.

Accepted for publication in *Monthly Weather Review*. DOI 10.1175/MWR-D-19-0038.1.

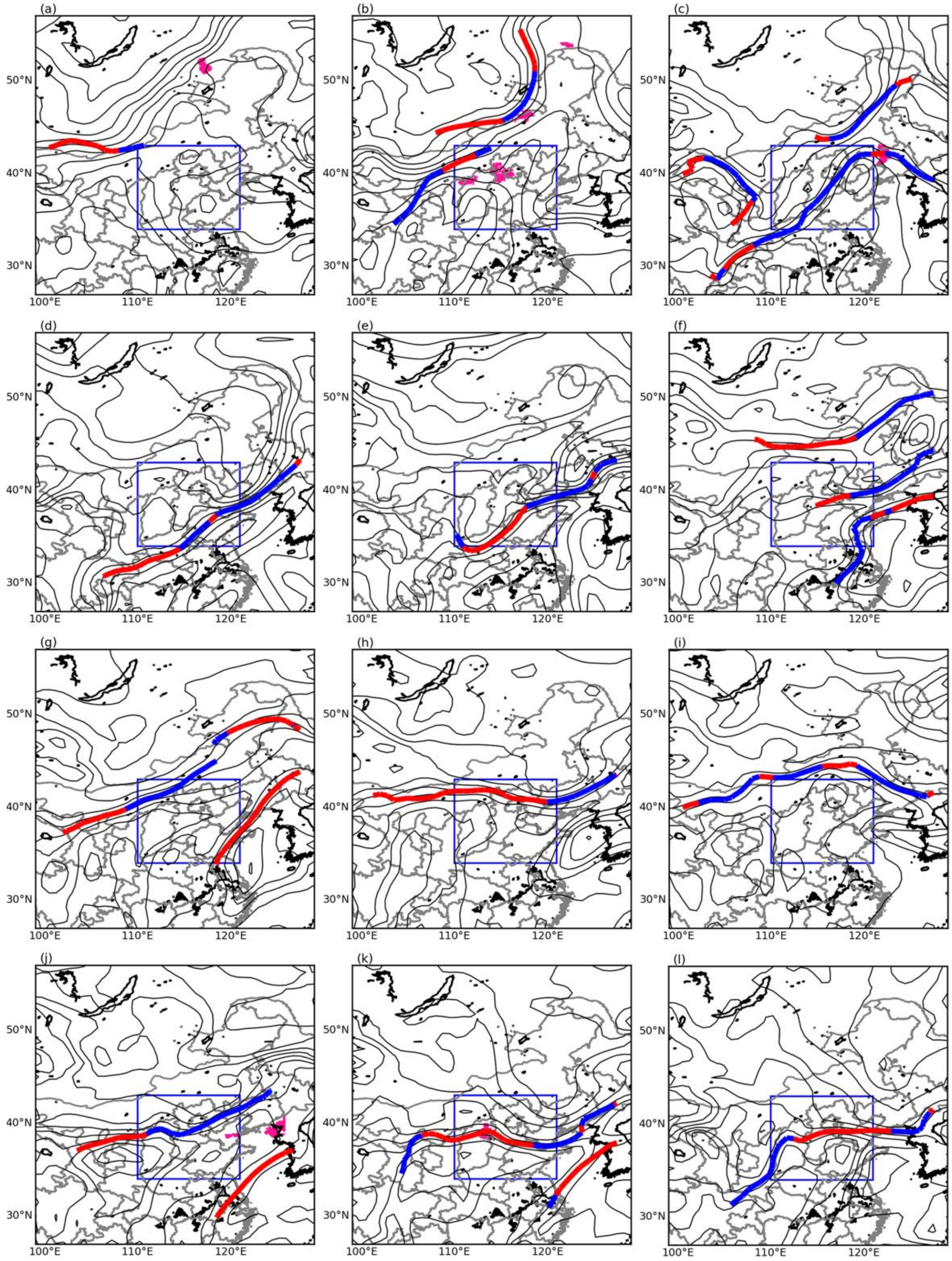

Fig.5 850hPa equivalent potential temperature (black contours, interval x4K) , identified front locations (blue/red lines) at 08:00 LST, and detected mesoscale rainstorms (pink shaded) at 13:00 LST during the period from 20th (a) to 31st (l) July 2012. The blue rectangle

Accepted for publication in *Monthly Weather Review*. DOI 10.1175/MWR-D-19-0038.1.

represents North China.

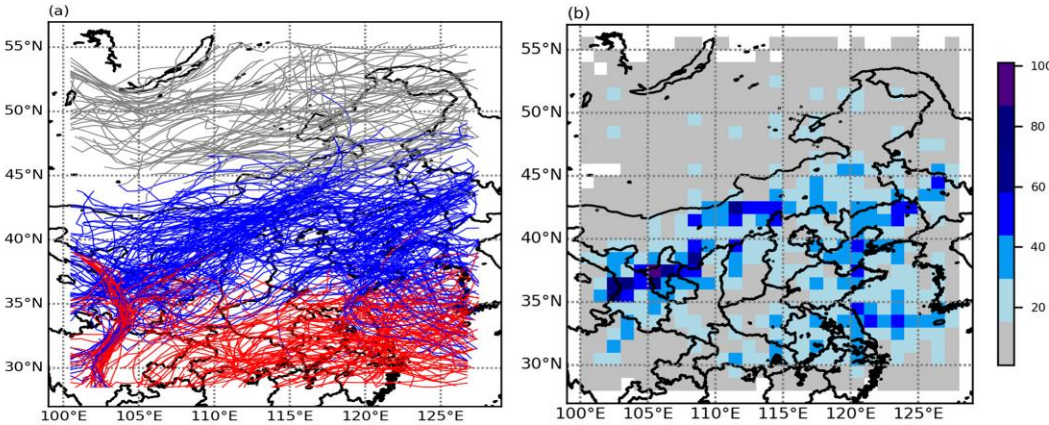

Fig.6 (a) The distribution of synoptic scale fronts for all detected warm sector rainstorms. Grey, blue and red lines indicate that fronts are averagely located at north of 45°N, between 35 and 45°N, south of 35°N, respectively. (b) Front frequency in one degree grid boxes during the period under study.

Accepted for publication in *Monthly Weather Review*. DOI 10.1175/MWR-D-19-0038.1.

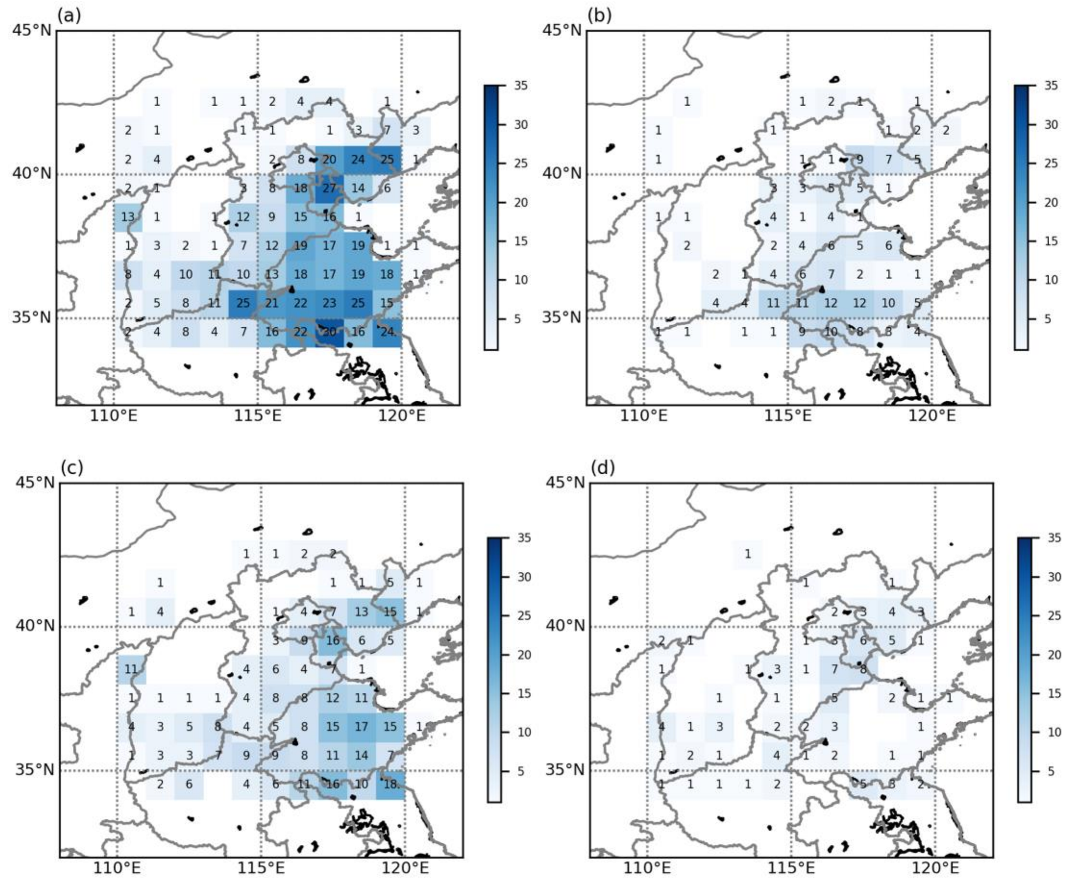

Fig.7 The distribution of warm sector rainstorms in North China for (a) June to September, (b) June 15 to July 14, (c) July 15 to August 14, and (d) August 15 to September 14, all for 2012 to 2017. Figures show actual values.

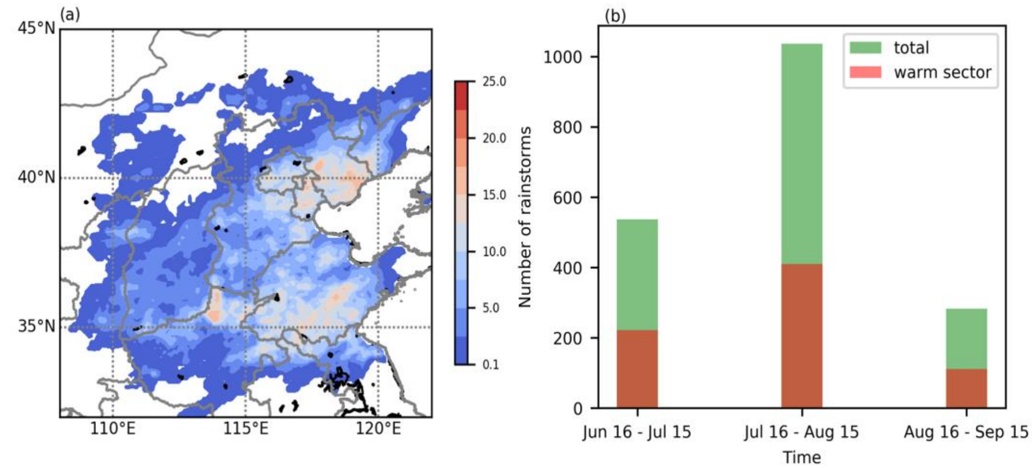

Fig.8 (a) Spatial distribution of the ratio (%) of rainfall attributable to warm sector rainstorm versus rainfall attributable to all rainstorms over North China during the study period, (b) frequencies of these rainstorm types by date.

Accepted for publication in *Monthly Weather Review*. DOI 10.1175/MWR-D-19-0038.1.

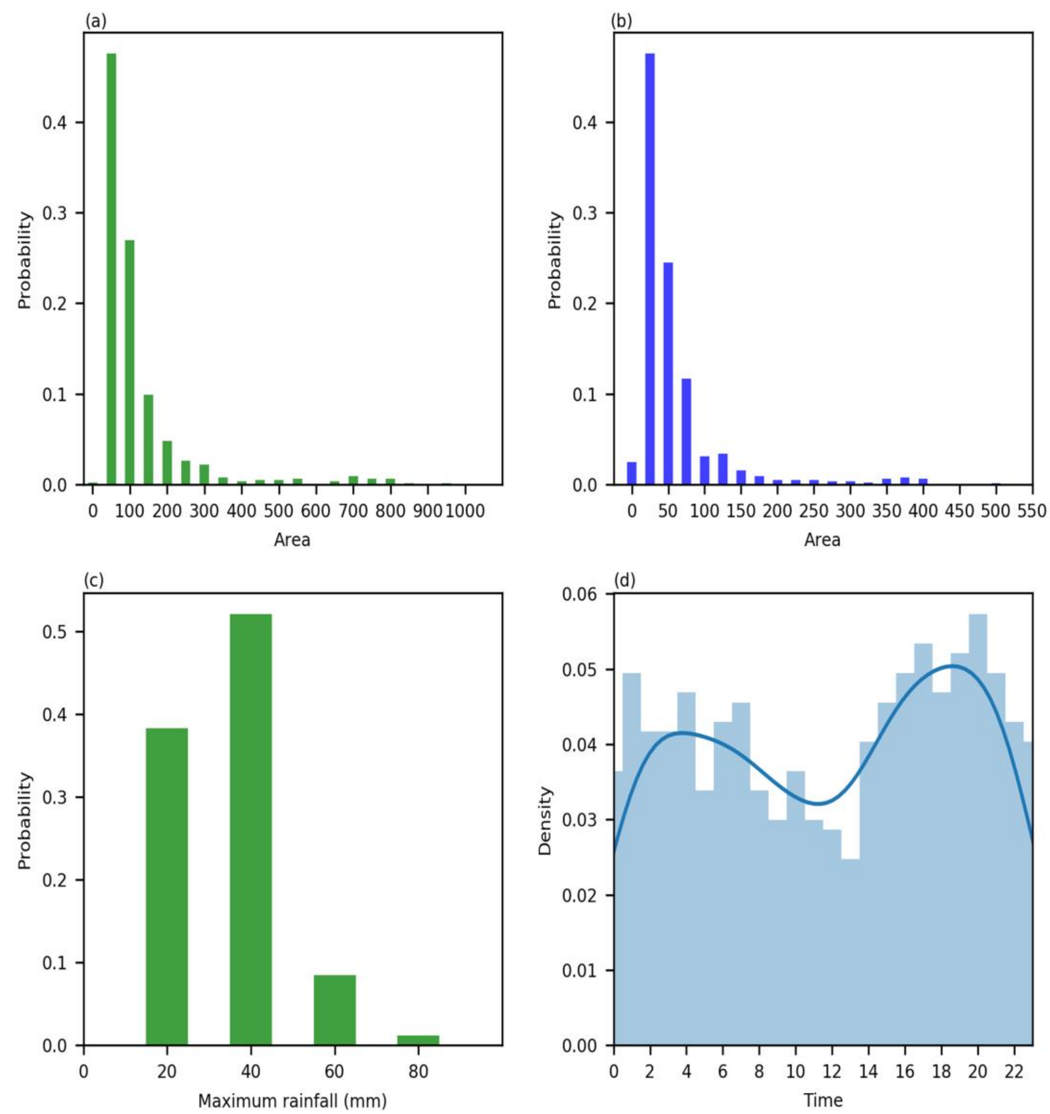

Fig.9 Warm sector rainstorm statistics for North China for the study period. (a) Rainstorm area (km^2), (b) area with rainfall larger than 10 mm in 1h (km^2), (c) maximum rainfall (mm in 1h), (d) times of occurrence.

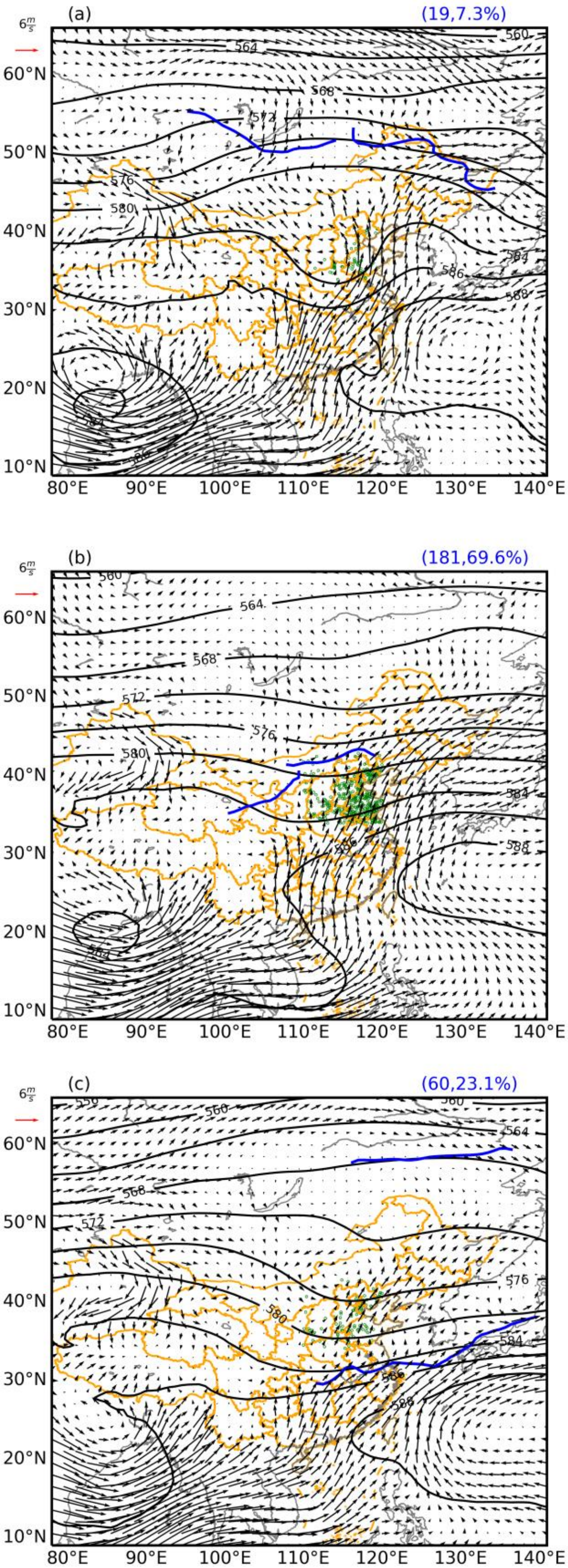

Accepted for publication in *Monthly Weather Review*. DOI 10.1175/MWR-D-19-0038.1.

Fig.10 Composite analysis of 500hPa geopotential height (unit: dm), 850hPa wind vectors and average front lines (blue) for three different circulation patterns. (a) Mongolian front pattern, (b) northern China front pattern, (c) southern front pattern. The numbers in brackets over each picture's upper right corner indicate the total numbers within the composite and the relative frequency of each synoptic pattern. The green dots are the centroids of rainstorms associated with each synoptic pattern.

Accepted for publication in *Monthly Weather Review*. DOI 10.1175/MWR-D-19-0038.1.

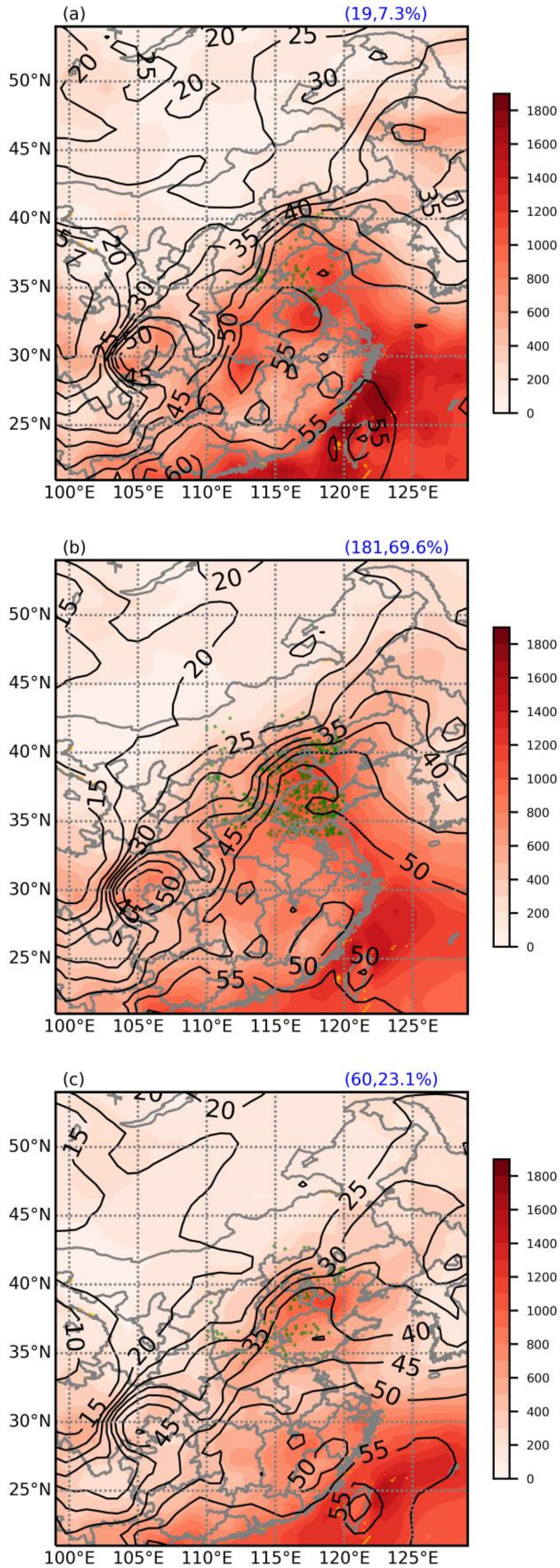

Accepted for publication in *Monthly Weather Review*. DOI 10.1175/MWR-D-19-0038.1.

Fig.11 AS Fig.10, but for total column water vapor (mm, contours) and convective available potential energy (J/kg, shading) without superimposing the average front boundaries.

Accepted for publication in *Monthly Weather Review*. DOI 10.1175/MWR-D-19-0038.1.

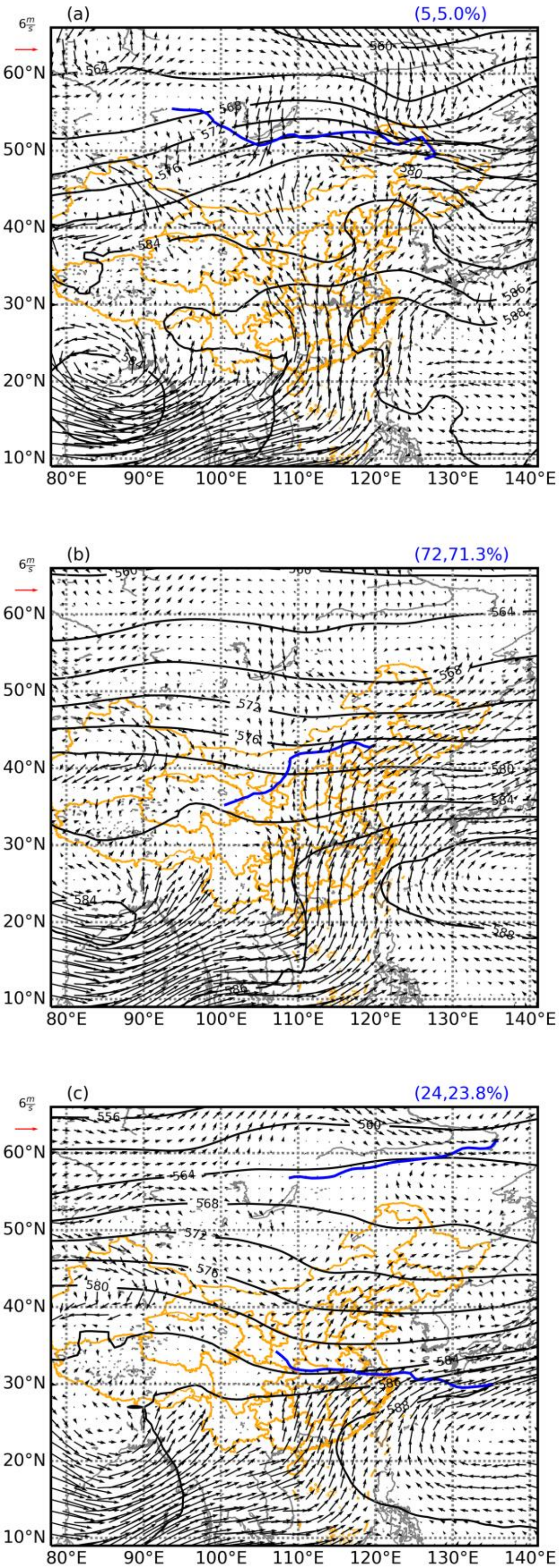
(a)
(5,5.0%)
(b)
(72,71.3%)
(c)
(24,23.8%)
60°N
50°N
40°N
30°N
20°N
10°N
80°E
90°E
100°E
110°E
120°E
130°E
140°E

Fig.12 As Fig.10, but for 6 hours ahead of the WSR-related rainstorms without superimposing their centroids. Also, for a continuous WSR event, only the circulations at the start of these events are composited.

Accepted for publication in *Monthly Weather Review*. DOI 10.1175/MWR-D-19-0038.1.

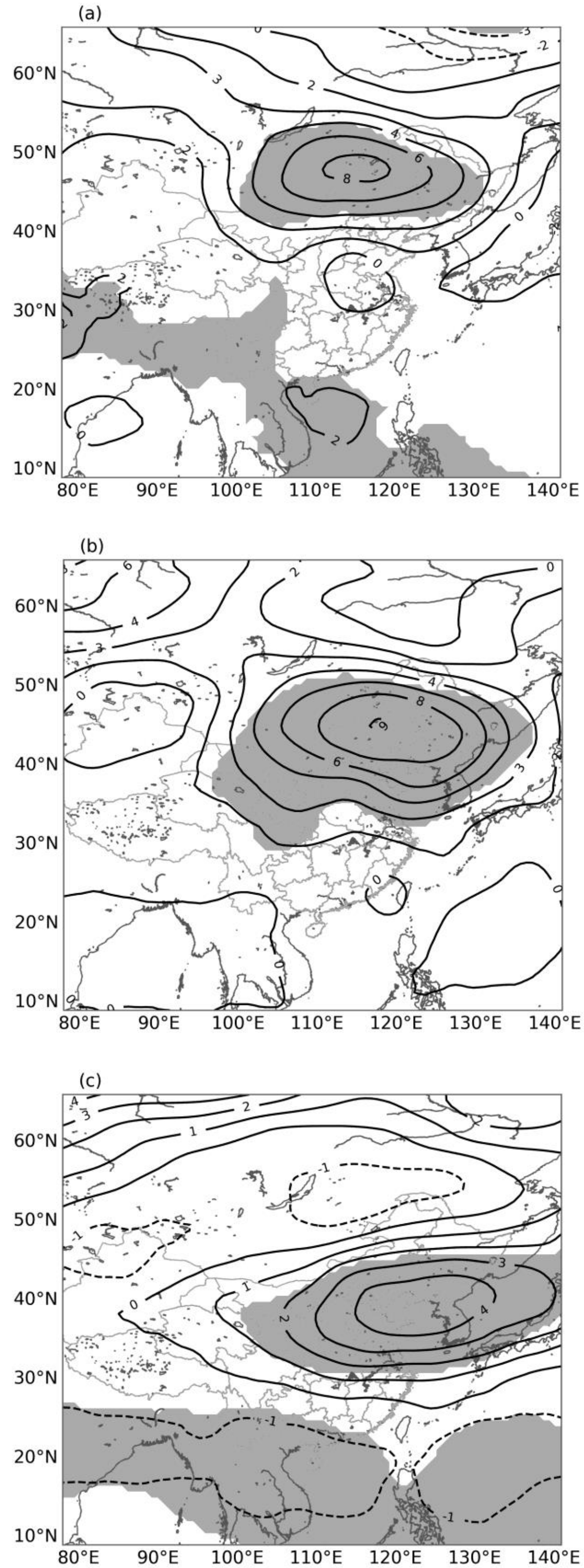

Accepted for publication in *Monthly Weather Review*. DOI 10.1175/MWR-D-19-0038.1.

Fig.13 The 500hPa height differences between Mongolia front and northern China front pattern（a）、Mongolia front and southern front pattern（b）、northern China front pattern and southern front pattern. Differences exceeding the 0.01 t test significant level are shaded.

Accepted for publication in *Monthly Weather Review*. DOI 10.1175/MWR-D-19-0038.1.